The EMBO Journal vol.11 no.4 pp.1607-1616, 1992

Subunit stoichiometry and three-dimensional arrangement in proteasomes from *Thermoplasma acidophilum*

Gabriela Pühler, Sevil Weinkauf[1], Luis Bachmann[1], Shirley Müller[2], Andreas Engel[2], Reiner Hegerl and Wolfgang Baumeister

Max-Planck-Institut für Biochemie, Am Klopferspitz, D-8033 Martinsried, [1]Technische Universität München, Lehrstuhl für Technische Chemie, Lichtenbergstrasse 4, D-8046 Garching, FRG and [2]Maurice E.Müller-Institut am Biozentrum der Universität Basel, Klingelbergstrasse 70, CH-4056 Basel, Switzerland

Communicated by W.Baumeister

The proteasome or multicatalytic proteinase from the archaebacterium *Thermoplasma acidophilum* is a 700 kDa multisubunit protein complex. Unlike proteasomes from eukaryotic cells which are composed of 10–20 different subunits, the *Thermoplasma* proteasome is made of only two types of subunit, α and β, which have molecular weights of 25.8 and 22.3 kDa, respectively. In this communication we present a three-dimensional stoichiometric model of the archaebacterial proteasome deduced from electron microscopic investigations. The techniques which we have used include image analysis of negatively stained single particles, image analysis of metal decorated small three-dimensional crystals after freeze-etching and STEM mass measurements of freeze-dried particles. The archaebacterial and eukaryotic proteasomes are almost identical in size and shape; the subunits are arranged in four rings which are stacked together such that they collectively form a barrel-shaped complex. According to a previous immunoelectron microscopic investigation, the α-subunits form the two outer rings of the stack, while the two rings composed of β-subunits, which are supposed to carry the active sites, are sandwiched between them. Each of the α- and β-rings contains seven subunits; hence the stoichiometry of the whole proteasome is $\alpha_{14}\beta_{14}$ and the symmetry is 7-fold. Image simulation experiments indicate that the α- and β-subunits are not in register along the cylinder axis; rather it appears that the β-rings are rotated with respect to the α-rings by $\sim 25°$. In contrast to some previous reports we have not been able to find stoichiometric amounts of RNA associated with highly purified proteolytically active proteasome preparations.

Key words: electron microscopy/image processing/multicatalytic proteinase/proteasomes/*Thermoplasma*

Introduction

Proteasomes are high molecular weight multisubunit complexes with at least three distinct proteolytic activities ('trypsin-like', 'chymotrypsin-like' and peptidylglutamyl-peptide hydrolysing) (for recent reviews see Rivett, 1989; Orlowski, 1990). They are highly conserved and ubiquitous in eukaryotic cells from yeast to man (Arrigo *et al.*, 1987, 1988; Falkenburg *et al.*, 1988). More recently, proteasomes were also found in the archaebacterium *Thermoplasma acidophilum* (Dahlmann *et al.*, 1989). Proteasomes are identical to the hollow cylinder protein or cylindrin, a major component of erythrocytes discovered many years ago by electron microscopy (Harris, 1968). They are also identical to prosomes, which are considered to be ribonucleoproteins involved in the control of gene expression (Scherrer, 1990; Schmid *et al.*, 1984) and the multicatalytic proteinase (Dahlmann *et al.*, 1985; Rivett, 1989), an abundantly characterized non-lysosomal proteinase. It is still a controversial issue, whether or not proteasomes are a component, perhaps the catalytic core, of the 26S complex thought to be responsible for the ATP-dependent proteolysis of ubiquitin-conjugated proteins (Hough *et al.*, 1988; Eytan *et al.*, 1989; Ishiura *et al.*, 1989; Driscoll and Goldberg, 1990). Furthermore, recent data indicate that the proteasome is related to the 'low molecular weight protein' (LMP) which has a subunit composition of similar complexity (Monaco and McDevitt, 1982, 1984). From mapping of corresponding genes to the MHC II region (Brown *et al.*, 1991; Glynne *et al.*, 1991), in close vicinity to putative peptide transporters, and from the transcriptional co-regulation of this gene cluster, it has been concluded that the LMP or the proteasome play a role in antigen processing (Parham, 1990).

Eukaryotic proteasomes have a rather complex subunit composition; they typically contain 10–20 distinctly different though related subunits, apparently encoded by one gene family (Fujiwara *et al.*, 1990; Haass *et al.*, 1990). Proteasomes from *T.acidophilum* have the same quarternary structure, i.e. the subunits assemble into four rings or discs, which collectively form the cylindrical or barrel-shaped complex (Hegerl *et al.*, 1991). However, the *T.acidophilum* proteasome consists of only two different subunits, α (25.8 kDa) and β (22.3 kDa) (Dahlmann *et al.*, 1989; Zwickl *et al.*, 1992). We have shown by immunoelectron microscopy that the α-subunits are located in the two outer discs of the proteasome, while the β-subunits, which we assume to be the catalytic subunits, constitute the two juxtaposed inner rings (Grziwa *et al.*, 1991). Since all of the eukaryotic subunits for which amino acid sequences are available so far fall into two classes, which can be related to either the α- or β-subunit of the *Thermoplasma* proteasome, it is quite likely that the α- and β-homologues occupy equivalent positions in the eukaryotic proteasome. It has not escaped our attention that the basic architecture of proteasomes has several features in common with molecular chaperones of the GroEL family of proteins (Zwickl *et al.*, 1990).

Because of its relatively simple subunit composition, the *Thermoplasma* proteasome is an attractive candidate for a detailed structure investigation. As we report in this communication, we have obtained three-dimensional crystals of *Thermoplasma* proteasomes. Although these crystals proved

unsuitable for X-ray diffraction analysis, electron microscopy of freeze-etched and metal decorated crystals (Bachmann *et al.*, 1989) provided valuable information about the arrangement of the subunits of proteasomes. Using scanning transmission electron microscopy (STEM) mass measurements (Engel, 1978) as a constraint, image stimulation allows a model for the subunit stoichiometry and arrangement in the complex to be proposed. In this context we have to address the controversial issue of an association of proteasomes with RNA. Some authors have reported that proteasomes (or prosomes) contain 10–15% RNA (Scherrer, 1990; Schmid *et al.*, 1984) others an even higher RNA content of up to 23% (Arrigo *et al.*, 1985). This would have a major impact on stoichiometric considerations.

Results

Purification of the Thermoplasma proteasome

With the new purification scheme described in Materials and methods, the yield of highly purified proteasomes has been increased 8-fold. Starting with 20 g (wet weight) of *Thermoplasma* cells, ~40 mg pure proteasomes were obtained, compared with the 5–6 mg obtained with the earlier purification procedure (Dahlmann *et al.*, 1989). Since proteasomes can only be lost in the course of the purification, this figure must be taken as a lower limit of the cytoplasmic content of proteasomes in these cells. Figure 1a shows an electron micrograph of a proteasome preparation obtained with the new purification scheme and an average projected structure (Figure 1c) based on ~2200 individual molecular images, which shows the molecule side-on. SDS–PAGE (Figure 1b) of purified protein reveals two bands with equal staining intensities and apparent molecular weights of 26 kDa (α-subunit) and 23 kDa (β-subunit) respectively.

RNA characterization

In order to examine the purported association of proteasomes with RNA, we have subjected proteasomes from different preparations to an RNA extraction procedure and characterized the radioactively labelled nucleic acid fractions on urea–polyacrylamide gels (Figure 2). Each lane on the autoradiogram represents the RNA content from equal amounts (20 μg) of proteasomes. In the control experiment, labelled extracts of eukaryotic proteasomes, purified from rat liver (Figure 2, lane 7) and rabbit muscle (Figure 2, lane 8) (Dahlmann *et al.*, 1985) were loaded onto the gel. Strong radioactive signals in the size range of 120 nucleotides (corresponding to the size of 5S rRNA) and several labelled species in the size range of 80 nucleotides (corresponding to the size of tRNA) were observed. A very similar pattern was obtained with extracts of the *T.acidophilum* proteasomes purified on a Mono Q column (Figure 2, lane 3). Proteasomes purified with the chromatofocusing column Mono P, however, showed less RNA in the size range of 80 nucleotides and no RNA in the size range of 120 nucleotides (Figure 2, lane 2).

Proteasomes incubated with 100 mM glycine, pH 2.6, are dissociated into individual subunits which reassemble upon

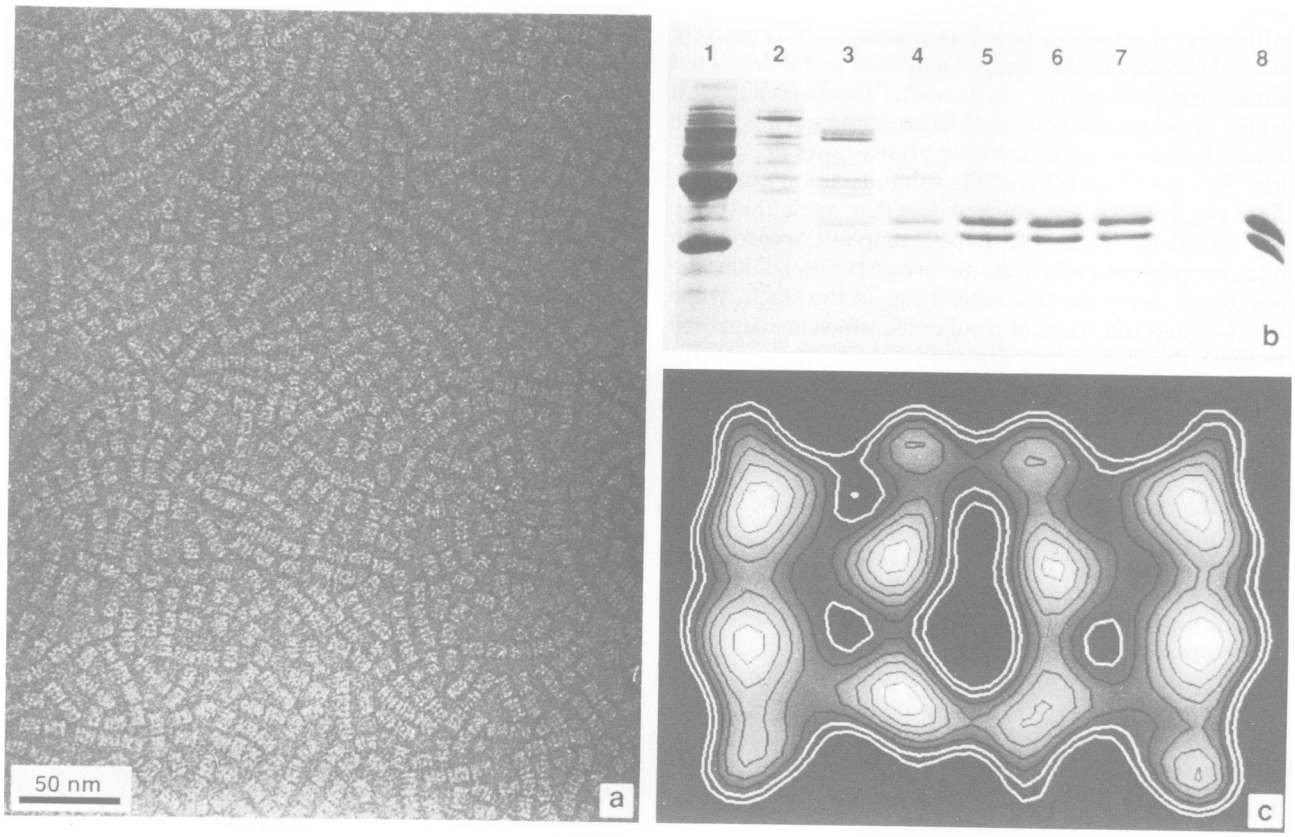

Fig. 1. Proteasomes from *Thermoplasma acidophilum* isolated using the new purification scheme: (**a**) Electron micrograph of negatively stained proteasomes; (**b**) Coomassie stained 16% SDS–PAGE from fractions of a 100 mM to 1 M potassium phosphate gradient run on a hydroxylapatite column: lane 1 proteins, which do not bind; lanes 2–4, fractions with high optical density of 280 nm and without 'chymotryptic' activity; lanes 5–7, purified proteasomes eluting at ~480 mM potassium phosphate showing 'chymotryptic' activity; lane 8, reference of purified proteasomes from a former preparation; (**c**) Average of proteasome side views based on ~2200 individual molecular images.

dialysis against 10 mM Tris–HCl buffer, pH 7.5. On electron micrographs the reassembled proteasomes are indistinguishable from native proteasomes and they were fully active (Grziwa *et al.*, in preparation). Extracted aliquots of dissociated (Figure 2, lane 5) and reassembled proteasomes (Figure 2, lane 6) were prepared (again corresponding to 20 μg proteasomes), radioactively labelled and run on a gel. After 12 h of exposure, no radioactive labelling was seen. Only little radioactive labelling was seen in extracts from dissociated proteasomes after several days of exposure (not shown). The same result (i.e. no detectable RNA even after prolonged exposure) was obtained when proteasomes from dissolved crystals (see below) were subjected to RNA extraction (Figure 2, lane 4).

STEM mass determination

Even at a low recording dose, STEM elastic dark field images of freeze-dried proteasomes revealed two characteristic views (Figure 3a and b). The particles were either rectangular [length 17.8 ± 1.6 nm (n = 19), width 11.4 ± 1.5 nm (n = 19)] or showed a circular cross section [diameter 11.3 ± 1.2 nm (n = 14)]. This corresponds to side and top views of the barrel-shaped proteasome (Hegerl *et al.*, 1991), which were also observed after negative staining. While the width of the side views and diameter of the top views coincide with those from negatively stained samples, the length is ~20% larger, suggesting that a significant fraction of side views were from freeze-dried particles whose axes were not perpendicular to the optical axis of the STEM. To determine the mass, the counts (i.e. number of electrons scattered onto the annular detector) within circular boxes positioned over the particles were integrated, the background from the carbon film subtracted and this difference normalized to the recording dose. Different box diameters were selected for side and top views (Figure 3b). The absolute mass scale was evaluated from the mass-per-length (MPL) values of co-prepared TMV. While variations in the TMV MPL [130 ± 12.6 kDa/nm, (n = 204)] resulted from differences of the specimen, the magnification and the recording dose, the proteasome mass values revealed a wider spread. In particular they exhibited a faster rate of mass loss than tobacco mosaic virus (TMV) within a dose range of 140–600 electrons/nm^2. Therefore, a series of mass measurements was made at doses between 140 and 220 electrons/nm^2, scaled with respect to TMV particles recorded at the same dose and fitted by a Gaussian profile, yielding 690 ± 90 kDa (n = 270; Figure 3c) for the particle weight of the proteasome. In addition, a linear regression was used to extrapolate the MPL value of TMV back to zero dose from data collected over a dose range between 140 and 600 electrons/nm^2. Taking this value to scale all proteasome masses, their mass loss kinetics were evaluated, and the proteasome mass was extrapolated linearly to zero dose, giving 703 ± 25 kDa (95% confidence limit, Figure 3d).

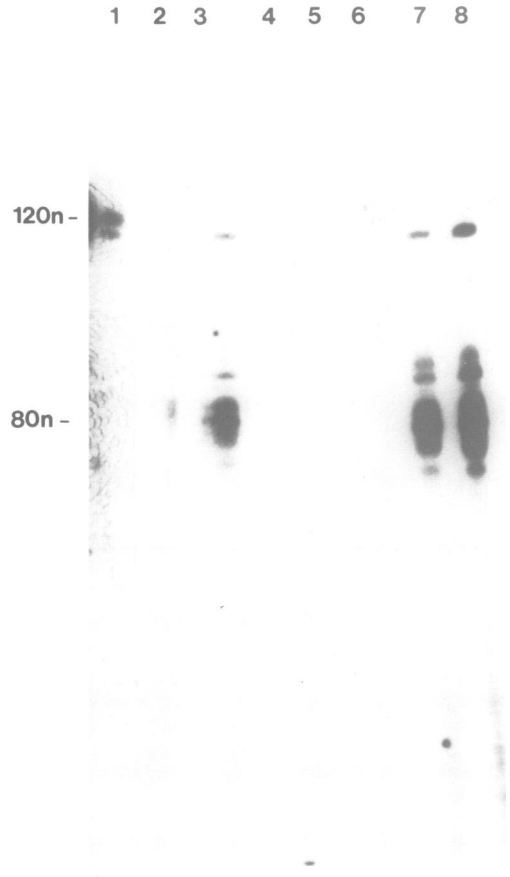

Fig. 2. Autoradiogram of 8% urea–PAGE (12 h exposure). Lane 1: 1 ng *E.coli* 5S rRNA. The following lanes show radioactively labelled RNA extracts corresponding to 20 μg proteasomes: lane 2, *T.acidophilum* proteasomes purified with Mono P; lane 3, *T.acidophilum* proteasomes purified with Mono Q; lane 4, *T.acidophilum* proteasomes from dissolved crystals; lane 5, *T.acidophilum* proteasomes dissociated by 100 mM glycine pH 2.6; lane 6, *T.acidophilum* proteasomes reconstituted from dissociated proteasomes by dialysis against 10 mM Tris–HCl buffer pH 7.5; lane 7, proteasomes from rat liver; lane 8, proteasomes from rabbit muscle. Eukaryotic proteasomes were kindly provided by B.Dahlmann. As size markers, *E.coli* 5S rRNA (120 nucleotides) and Phe-tRNA (80 nucleotides) were used.

Freeze-etching of proteasome crystals

Using the crystallization conditions described in Materials and methods, we reproducibly obtained three-dimensional crystals, ranging in size from several micrometres to 0.4 mm. Two different crystal forms were found to coexist in single droplets: thin, apparently hexagonal platelets and elongated prisms. While the morphologically more regular prisms did not diffract, the hexagonal platelets were too small for X-ray diffraction. Therefore, we have used electron microscopy to examine replicas of platinum/carbon shadowed crystal surfaces to deduce some structural parameters. Figure 4 shows replicas of the predominant crystal planes revealed by freeze-etching.

The plane displayed in Figure 4a shows the individual proteasomes end-on. At a first glance it appears as if the proteasomes were hexagonally packed, but closer inspection of the optical transform tells otherwise. Figure 4e and h show the individual proteasomes side-on, but the corresponding lattice constants are different (see Table I). As yet it cannot be decided whether these micrographs show planes of the same crystal form with different indices or belong to different crystal packing arrangements. An unequivocal assignment of the observed planes and their correct indexing would require a knowledge of the space group(s). Correlation averages from micrographs of the three crystal planes shown in Figure 4a, e and h provide reliable data regarding the proteasome dimensions and their packing in the crystal (Figure 4c, d, g and j; see also Table I). It is obvious from the averages of the two adjacent crystal planes showing the

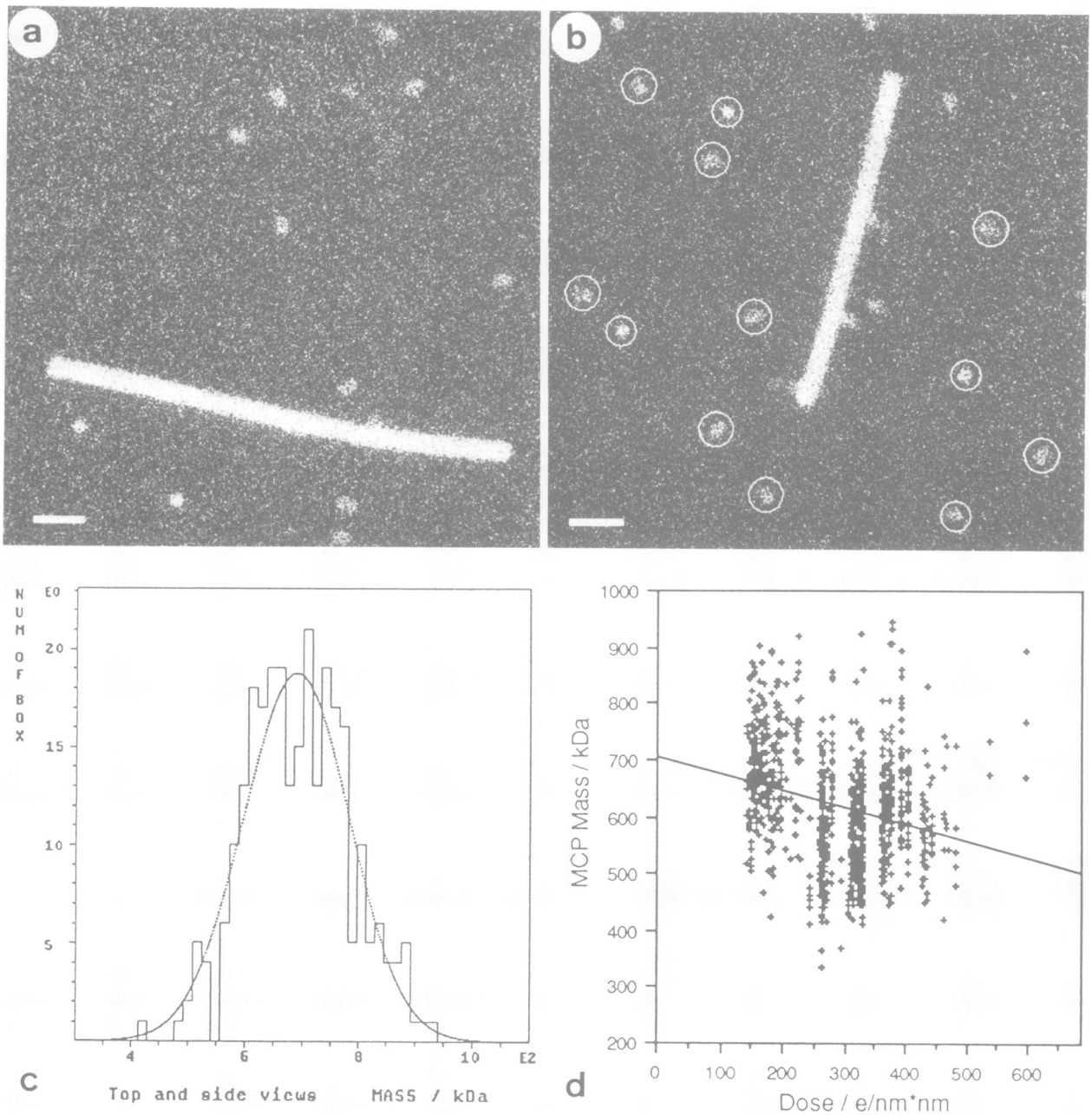

Fig. 3. STEM mass determination: Proteasomes and TMV particles were adsorbed to thin carbon film, extensively washed and freeze-dried. (**a**) Low dose elastic dark-field images revealed either round and bright or rectangular and somewhat less bright particles. (**b**) Two types of circular boxes were used to determine the mass of these particles, identified as top and side views of the barrel-shaped proteasomes. TMV (300 nm long rods in panels a and b, bar corresponding to 50 nm) was used as an internal mass standard. (**c**) One set of proteasome mass values from dark-field images recorded at 140–220 electrons/nm^2 was fitted with a Gaussian profile to evaluate mean and standard deviation (690 ± 90 kDa). (**d**) Small particles such as proteasomes exhibit a significant mass loss during electron irradiation. A linear extrapolation to zero dose allows the initial mass to be estimated.

proteasome end-on (Figure 4a), that the molecules are arranged on an orthorhombic and not on a hexagonal lattice (Figure 4c and d). The diameter of individual proteasomes is close to 11 nm. The long axes of the surface lattices of the two other planes shown in Figure 4g and j are 58.1 and 28.1 nm respectively, The proteasomes are seen side-on with their cylinder axis parallel to the long axis of the surface lattice; the lattice with the longer lattice constant accommodates four proteasomes (Figure 4g), the lattice with the shorter lattice constant two (Figure 4j). Hence the length of a proteasome must be in the range 14.0–14.5 nm. The averages further indicate that the orientation of the proteasome in the unit cell alternates due to a rotation around the cylinder axis. The dimensions derived from the three-dimensional crystals are in excellent agreement with results of previous measurements performed with individual negatively stained proteasomes (Baumeister *et al.*, 1988; Dahlmann *et al.*, 1989).

Metal decoration is capable of detecting surface structures, which cannot be resolved by metal shadowing. Topological as well as topochemical effects govern the distribution of the metal clusters on the protein surface (Weinkauf *et al.*, 1991). Decoration reveals molecular symmetries and it allows the orientations of the individual molecules in a lattice

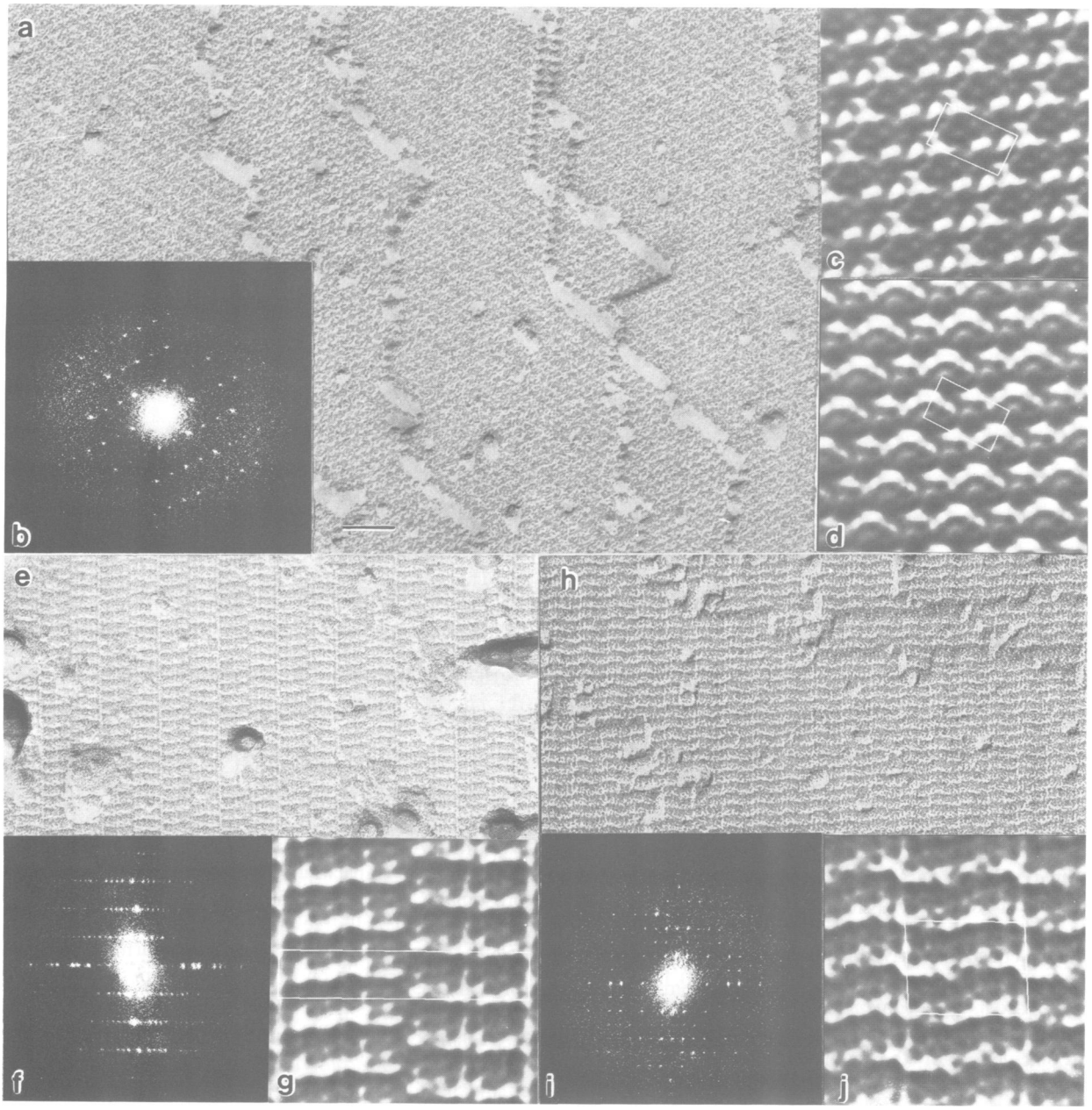

Fig. 4. Different planes of proteasome crystals, deep-etched and shadowed with platinum/carbon (1.5 nm), showing the proteasomes in end-on (**a**) and side-on orientations (**e** and **h**) with corresponding optical diffractograms (**b**, **f** and **i**). The bar in panel a corresponds to 50 nm. Averages obtained by CAV from platinum/carbon-shadowed surfaces of proteasome crystals are shown in panels **c**, **d**, **g** and **j**. Unit cells are marked with white boxes. The lattice parameters are summarized in Table I. (c) and (d): Surfaces with proteasomes in the end-on orientation obtained from two neighbouring planes of the same crystal surface. (g) and (j): Surfaces of two different crystal forms both showing the proteasomes in side-on orientation.

Table I. Lattice parameters of different planes of proteasome crystals

Type of surface lattice	Figure	Preparation[a]	(2D) Lattice parameters			Orientation of proteasomes
			a (nm)	*b* (nm)	α (°)	
I	6c	Pt/C	10.7	10.7	60.3	end-on
	6d	Au	11.2	11.1	57.9	end-on
II	4c	Pt/C	18.1	10.5	88.5	end-on
	4d	Pt/C	17.7	10.3	91.9	end-on
	5c	Au	19.1	10.1	87.5	end-on
III	4j	Pt/C	28.1	21.6	87.3	side-on
IV	4g	Pt/C	58.1	11.0	90.0	side-on

[a]Pt/C: platinum/carbon shadowing; Au: gold decoration.

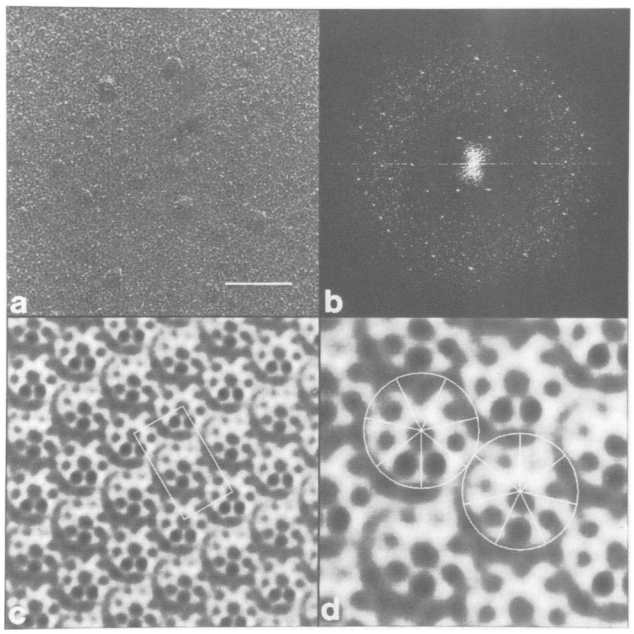

Fig. 5. Surfaces of a proteasome crystal with the molecules in end-on orientation and decorated with gold clusters. The gold sites of decorated crystals in the images appear dark. (**a**) Subframe of the original micrograph (bar corresponds to 50 nm). (**b**) Corresponding power spectrum of micrograph panel a. (**c**) Average of (a) with the unit cell indicated by a white frame. (**d**) Central area of (c) magnified by a factor of two. The superimposed circles with the seven subdivisions reflect the symmetry and show that neighbouring proteasomes differ in orientation; they are rotated with respect to each other by an angle of 25°.

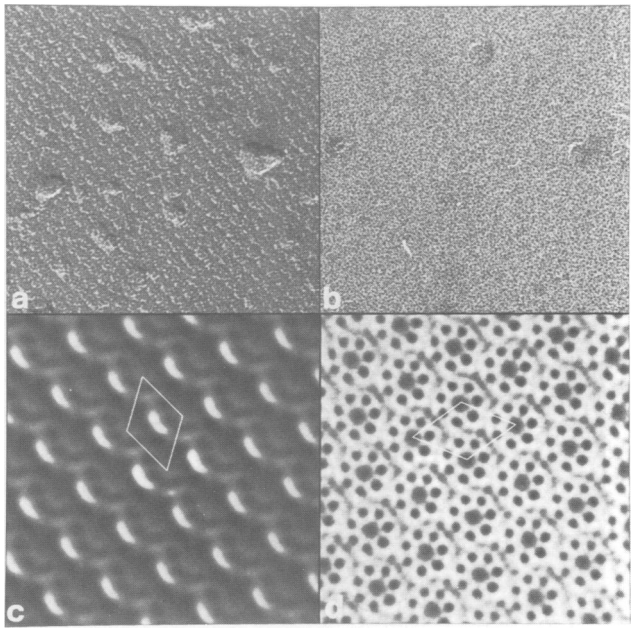

Fig. 6. A different (pseudohexagonal) crystal form, also showing the proteasomes end-on. (**a**) Subframe of a micrograph of a replica produced with platinum/carbon shadowing. (**b**) Subframe of a micrograph of a replica produced with gold decoration. (**c**) Average of the micrograph shown in (a). (**d**) Average of the micrograph shown in (b). Unit cells are indicated by superimposed frames. The 7-fold symmetry of the proteasomes is clearly revealed by decoration with gold.

to be determined (Bacher,A., Weinkauf,S., Bachmann,L., Ritsert,K., Baumeister,W., Huber,R. and Ladenstein,R., submitted). Figure 5a shows a gold-decorated plane of a proteasome crystal. Due to the normal incidence of the evaporated gold, the individual molecules are hardly visible. The lattice constants derived from the computed diffraction patterns (Figure 5b; a = 19.1 nm, b = 10.1 nm and α = 90°) are in close agreement with the lattice parameters in Figure 4c and d, indicating that the direction of observation coincides with the cylinder axis and individual proteasomes are seen end-on. The corresponding average shows eight distinct decoration sites for each proteasome (Figure 5c and d). Seven of these are arranged in a ring with a radius of ~3.8 nm around the eighth site; neighbouring proteasomes differ in orientation (Figure 5d). This strongly suggests that at least the outer 'discs' of the proteasome, which are made of the α-subunits, have 7-fold symmetry. The fact that the seven decoration sites appear non-equivalent may be ascribed to some residual 'shadowing' due to the carbon backing in the course of replication. We found a second crystal plane, in shadowing as well as in decoration experiments (Figure 6a and b), with end-on views of the proteasomes. Here lattice constants were $a = b$ = 10.7 nm and α = 60.3°; neighbouring proteasomes appear identical in orientation (Figure 6c and d). The decoration pattern on individual proteasomes is identical to that in Figure 5, thus corroborating the 7-fold symmetry of the particle (Figure 6d).

Discussion

The association of proteasomes with RNA, whether functional or futile, is a controversial issue. The protagonists of the prosome concept regard small RNA species in the size range 50–150 nucleotides as intrinsic and essential components. The prosomal RNAs are assumed to hybridize with mRNA and, via this association, to play a role in the regulation of translation (Scherrer, 1990). *In vitro*, the prosomal RNAs have been shown to associate with mRNA and to inhibit cell free protein synthesis (Horsch *et al.*, 1989). Prosomes, which are usually purified by sucrose gradient centrifugation, have been reported to contain 10–15% of RNA; this corresponds to one to two RNA molecules per complex. Except for the partial sequencing of a small RNA species from *Drosophila* prosomes (Arrigo *et al.*, 1985), which turned out to be homologous to the U6 mammalian small nuclear RNA, no further characterization of prosome or proteasome associated RNA species has been reported.

Amongst those who consider proteasomes to be primarily a multicatalytic proteinase, some have found RNA associated with their preparation of the complex (Falkenburg *et al.*, 1988) while others have stated explicitly that they were unable to detect any RNA (Arrigo *et al.*, 1988). No RNA was found associated with the 22S cylinder particle of *Xenopus laevis* (Kleinschmidt *et al.*, 1983), which is also regarded to be identical with the proteasome.

Recently Skilton *et al.* (1991) undertook a careful investigation of the RNA content of proteasomes by comparing different preparation protocols with regard to the copurification of small RNA species. Although one major RNA species of ~80 nucleotides turned out to co-purify with all preparations, these authors came to the conclusion that the association is sub-stoichiometric, i.e. the amount of RNA is less than one molecule per proteasome. Schliephacke *et al.* (1991) arrived at a similar conclusion for plant proteasomes.

Our results confirm that RNA tends to co-purify with proteasomes. The RNA species we found to be associated

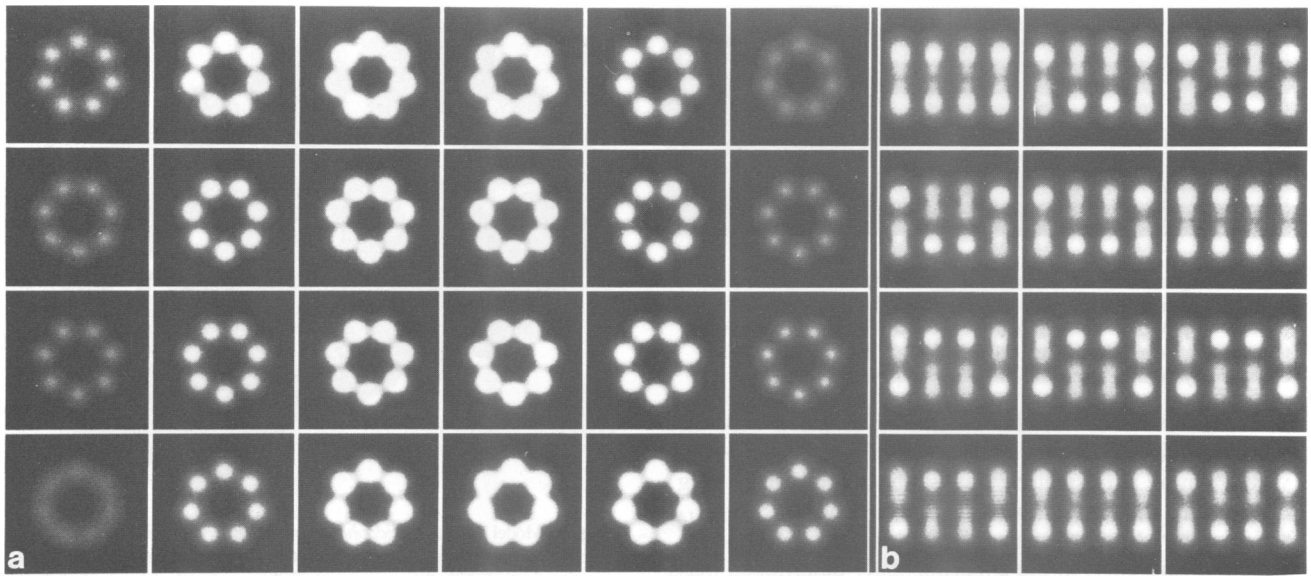

Fig. 7. (a) Models were generated by stacking together four rings each of seven spherical subunits rotating the two inner rings with respect to the outer rings. In the model shown here in the form of sections perpendicular to the cylinder axis and ~0.63 nm apart, the inner rings (second and third row) are rotated by 25.7° with respect to the outer rings, thus bringing them maximally out of register. (b) A sequence of side-on projections calculated from the model displayed in (a). Subsequent projections (from top left to bottom right) correspond to the model rotated around the cylinder axis with increments of 5.14°.

with the archaebacterial proteasome are similar in size to those described for eukaryotic proteasomes (80 and 120 nucleotides in length). However, even minor changes in the preparation protocol, such as the use of a Mono P column instead of a Mono Q column, drastically changed the amount of co-purifying RNA. In fact, the proteasome preparations of the highest purity, i.e. the reconstituted proteasomes and proteasomes from dissolved three-dimensional crystals, contained no detectable RNA at all. The sensitivity of our assay should allow us to detect as little as 1 ng RNA (see Figure 2, lane 1) (corresponding to 30 fmol of 100 nucleotide long single-stranded RNA). Assuming an RNA:protein ratio of 1:1000 we would expect that in 20 μg proteasomes (M_r 680 000, 20 μg correspond to 29.4 pmol) there would be ~1 ng (30 fmol) RNA. From this we conclude that RNA is required neither for the assembly of proteasomes nor for maintaining their structural integrity nor for the enzymatic (i.e. proteolytic) activity of the complex. We cannot completely rule out the possibility that there is a transient RNA–proteasome association that is specific and of functional relevance, although this is not very likely. It is clear, however, from our data, that the RNA does not need to be taken into account in stoichiometric considerations.

STEM mass values of proteasomes exhibited a significantly larger variation than expected from straightforward statistical considerations (Wall and Hainfield, 1986). The low mass values measured may be explained by a dissociation of proteasomes due to the extensive washing required for residual salt removal. On the other hand, high mass values may be the result of low-molecular weight species trapped in the inner compartments of barrel-shaped proteasomes (Hegerl *et al.*, 1991). In addition, the significant electron dose-induced mass loss necessitated that data be recorded at doses <200 electrons/nm^2. This resulted in very noisy images on which the presence of extraneous matter or partial damage of proteasomes could not be detected. Images were also recorded at higher doses and the mass data linearly extrapolated to zero dose, using the extrapolated zero dose value of TMV MPL to scale the proteasome mass data to the best possible precision. 95% confidence limits for the TMV calibration measurements were ±3%, whereas those for the proteasome zero dose mass were 703 ± 25 kDa, yielding a 95% confidence limit of ±32 kDa for the absolute mass value. The assumption of linear mass loss kinetics is a rough approximation. Nevertheless, the data set recorded at doses of 140–120 electrons/nm^2 revealed a Gaussian distribution of proteasome masses at 690 ± 90 kDa (n = 270), corroborating the value obtained by linear extrapolation.

Table II. Possible subunit stoichiometries

Stoichiometry	Calculated M_r
$\alpha_{16}\beta_{16}$	769.6
$\alpha_{14}\beta_{14}$	673.4
$\alpha_{12}\beta_{12}$	577.2
$\alpha_{14}\beta_{12}$	628.8
$\alpha_{12}\beta_{14}$	621.8

The α (233 amino acid residues) and β (203 amino acid residues) subunits have M_r 25.8 and 22.3 kDa respectively.

Early models pictured the proteasome as a cylindrical stack of four rings made of six subunits each (Kopp *et al.*, 1986). Taking the molecular mass of the α- and β-subunits derived from the primary structure (Zwickl *et al.*, 1992) such an $\alpha_{12}\beta_{12}$ stoichiometry would give a total mass of 577.2 kDa (Table II), which is substantially less than the experimentally determined mass of ~700 kDa. Averaged images of negatively stained proteasome preparations—albeit difficult to interpret because of stain-level effects and superposition of features—already indicated that the particles might have a 7-fold symmetry (Dahlmann *et al.*, 1989; Zwickl *et al.*, 1990). The gold decoration experiments documented in this communication depict the 7-fold symmetry very clearly. Strictly, decoration reveals only surface features and therefore these images establish the 7-fold symmetry only for the outer rings made of the α-subunits, while we have

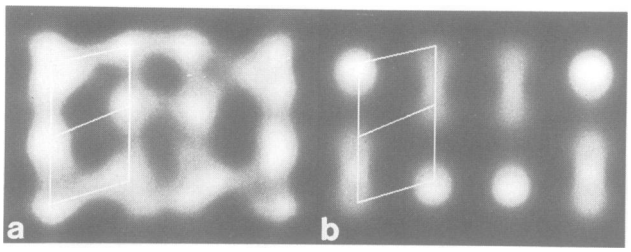

Fig. 8. Comparison of real projection data with the model. (**a**) Side-on view of a *T.acidophilum* proteasome obtained by single particle averaging. (**b**) Side-on projection of the model presented in Figure 9 (corresponding to a rotation around its cylinder axis of 12.9°). Centres of mass are connected by lines to emphasize the similarity positions.

no direct evidence for the symmetry of the β-subunits. However, since different symmetries of the α- and β-rings would cause a mismatch, any such stoichiometry (e.g. $\alpha_{14}\beta_{12}$) is unlikely. On the other hand an '$\alpha_{14}\beta_{14}$' stoichiometry has a calculated molecular mass of 673.4 kDa, which is very close to the experimentally determined mass (see Table II). We therefore assume that all four rings are made of seven subunits and that the particle probably has 7-fold symmetry.

Once the symmetry and the subunit stoichiometry are established, the remaining question to be settled is the relative arrangement of the α- and β-rings. To this end we have performed model calculations. Four rings of seven spherical subunits each were stacked together and projections perpendicular to the cylinder axis were calculated. These calculated side views were compared with averages of proteasomes in this orientation to find the best match. The modelling allowed the two outer and the two inner rings to be rotated with respect to each other and it also allowed us to change the orientation of the particle with respect to a virtual specimen support by rotating the model as a whole around the cylinder axis.

In configurations where all subunits are in register when viewed along the cylinder axis, obviously all four rings must produce the same pattern in any side-on projection. This is in conflict with the experimental data, showing essentially the same pattern for the two outer rings but a different one for the two inner rings. Rotating the two inner rings against the outer rings by an angle of 25.7° (= 360/14) thus bringing them maximally out of register (Figure 7a), produces the set of projections shown in Figure 7b. While some of the projections (0°, 25.7°, 51.4° etc.) show basically the same pattern for all four rings, most of the projections show a different behaviour corresponding quite well with the experimental data. Figure 8 compares an averaged image of a proteasome side view with one of the projections of the model. The dispositions of the centres of mass agree remarkably well. We therefore assume that the α- and β-rings are not in register with each other. A closer match can hardly be expected, since the use of ideally spherical subunits can only be regarded as a rough approximation of their real shape. Each subunit is, of course, a chiral entity and nothing is known about their orientation in the complex. The model shown in Figure 9 incorporates the previous assignment of the α- and β-subunits to the outer and inner rings based on immunoelectron microscopy (Grziwa *et al.*, 1991) with the stoichiometric considerations presented in this paper and with the spatial arrangement of the subunits deduced from the modelling experiments. It should be emphasized that this

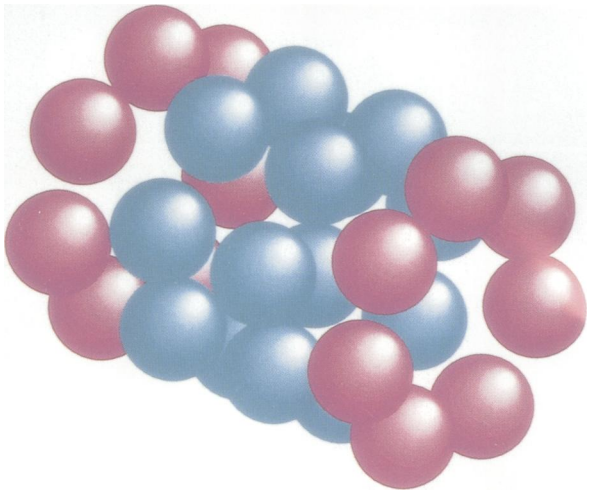

Fig. 9. Model of the *T.acidophilum* proteasome. Combining information about the arrangement and stoichiometry of the subunits detailed in this communication with the assignment of the α-subunits (shown in red) to the outer and of the β-subunits (shown in blue) to the inner rings as determined by immunoelectron microscopy (Grziwa *et al.*, 1991). The cylinder is 15 nm long, and 11 nm in diameter. The real shape of the subunits will deviate significantly from the spheres used to construct this model; this allows a more closed barrel-shaped structure to form, as revealed by the three-dimensional reconstruction of individual proteasomes (Hegerl *et al.*, 1991).

model only indicates the spatial disposition of the subunits. The model is radically different from the models put forward by Tanaka *et al.* (1988); from visual inspection of electron micrographs of proteasomes negatively stained with uranyl acetate, these authors concluded that the proteasome is a ring-shaped particle 16 nm in diameter and 11 nm in height with a hole of 1–3 nm diameter. We have shown previously that uranyl acetate tends to destabilize proteasomes and creates highly variable and aberrant shapes (Baumeister *et al.*, 1988). The dimensions Tanaka *et al.* (1988) found deviate substantially from measurements performed with single particles (Kopp *et al.*, 1986; Baumeister *et al.*, 1988; Dahlmann *et al.*, 1989) or of the proteasome dimensions derived from three-dimensional crystals as reported in this communication. On the other hand, Tanaka *et al.* (1988) have deduced a model from X-ray scattering experiments picturing the proteasome as a 'prolate ellipsoidal' structure with an ellipsoidal cavity in the centre; the long axis of this ellipsoid is 11.5 nm and the short axis is 5.75 nm. We have calculated a theoretical scattering function for the model (data not shown). This function fits the experimentally measured scattering profile as well as the model put forward by Tanaka *et al.* (1988). The measured radius of gyration is 6.59 nm, the calculated radius of gyration for our model is 6 nm. Therefore the deduced model, but not the experimental X-ray scattering data, of Tanaka *et al.* (1988) is in conflict with our model.

Materials and methods

Purification of proteasomes from T.acidophilum

Two methods were used to isolate and purify the proteasomes. The first basically followed the protocol described by Dahlmann *et al.* (1989) except for an ammonium sulphate precipitation step (0–40% and 40–80% saturation) introduced after centrifugation at 100 000 *g*. The 40–80% fraction was loaded on a Sepharose 6B gel filtration chromatography column. In one preparation, instead of FPLC ion exchange chromatography with

Mono Q (Pharmacia, Uppsala), a Mono P chromatofocusing column (Pharmacia, Uppsala) was used. In this case, the protein was loaded on the bis-Tris buffered column (25 mM [bis(2-hydroxyethyl)imino-tris(hydroxylmethyl)methane]), pH 6.3; Sigma) and eluted with a pH gradient ranging from pH 6.3 to 5.0 with polybuffer 74 (Pharmacia, Uppsala). The proteasomes eluted as expected at pH 5.4.

We developed another preparation scheme which increased the yield and the purity of proteasome significantly. Following chromatography on the Sepharose 6B column (see above) those fractions showing 'chymotryptic activity' (assayed with Suc-Ala-Ala-Phe-7-amino-4-methyl-coumarin, Bachem), with proteins in the high molecular weight range (~500–1000 kDa) were loaded on an ion exchange column prepared with DEAE–Sephacel (Pharmacia, Uppsala). Proteins were eluted with an NaCl gradient (0–500 mM) and the proteasome-containing fractions were then loaded directly, i.e. without dialysis, onto a hydroxylapatite affinity column (Bio-Rad). The column was equilibrated with 100 mM potassium phosphate buffer, pH 7.5. Proteasomes were eluted with a potassium phosphate buffer gradient from 100 mM to 1 M potassium phosphate. The proteasomes, which elute at a potassium phosphate concentration of 480 mM, were then dialysed against 3 mM MOPS buffer, pH 7.5.

Protein concentration was determined by the bicinchonic acid method (Sigma) as described by Smith *et al.* (1985). SDS–PAGE was performed as described elsewhere (Schägger and von Jagow, 1987).

RNA extraction, labelling and detection

Proteasomes purified with Mono Q or Mono P were incubated for 1 h at 37°C with 1 mg/ml proteinase K (Boehringer) and 0.1% SDS (Dineva *et al.*, 1989). RNA was extracted three times with phenol [Tris–HCl (pH 8.0) saturated phenol] followed by three extractions with chloroform–isoamyl alcohol. The extract was precipitated with ethanol. 3′-ends of RNAs were labelled with [^{32}P]pCp (Amersham, 300 Ci/mmol) in a reaction catalysed by T4, RNA ligase (Pharmacia, Uppsala) as described by England and Uhlenbeck (1987). Labelled RNAs were loaded on 8% urea–polyacrylamide gels (Maniatis, 1982). Separated RNAs were visualized by autoradiography on Trimax XM 3 M films. The exposure time at −70°C was ≥12 h. Radioactively labelled Phe-tRNA (Boehringer) and 5S rRNA (Boehringer) from *E.coli* were used as size markers.

Mass determination by STEM

For STEM mass measurements (Engel, 1978), proteasomes were adsorbed onto a thin, glow-discharge treated carbon film supported by a fenestrated film mounted on 200 mesh copper grids. TMV was added as an internal mass standard. After an adsorption period of 1 min, the grids were thoroughly washed in three droplets of quartz-distilled water with a blotting step between each wash. The sample was quickly frozen in liquid nitrogen, transferred to a freeze-drying chamber directly attached to the STEM and freeze-dried overnight at −90°C. Elastic scattering dark-field images, 512 × 512 pixels in size, were recorded in digital form at doses ranging between 100 and 800 electrons/nm^2 using a model HB-5 vacuum generator STEM operated at 80 kV and 200 000× nominal magnification (pixel size 1.05 nm). Processing of the STEM data from mass determination was carried out as described (Engel, 1978; Engel and Reichelt, 1988). Mass versus doses analysis was done by linear regression exercising the StatView programm implemented on a Macintosh.

Crystallization of purified proteasomes

Purified proteasomes in 3 mM MOPS buffer pH 7.5 (Serva) were concentrated in microconcentrators (Centricon-30, Amicon) up to a protein concentration of 10 mg/ml. Three parts of protein were mixed with one part of 10% polyethylene glycol (PEG 6000, Serva), 0.2 M phosphate buffer pH 8.0. The crystallization was carried out by the 'hanging drop method' and a reservoir solution (0.2 M sodium phosphate buffer, pH 8.0) at 4°C through vapor diffusion.

Freeze-etching, shadowing and decoration of proteasome crystals

For freeze-etching experiments, 'hanging droplets' containing small crystals of proteasomes (20–50 μm) were collected. The crystal suspension was concentrated by gentle centrifugation and washed twice with buffer containing 0.3 M sodium/potassium phosphate pH 8.0 and 15% PEG. Small droplets (1–2 μl) were transferred onto Balzers specimen mounts, frozen in liquid nitrogen to promote the growth of micrometre-sized ice crystals, and then fractured and deep-etched for 2–3 min at −100°C in a Balzers freeze-etching unit BA 360 or BAT 400T.

Shadowing with platinum/carbon or tantalum/tungsten was performed at 45° incidence angle using an electron beam evaporator. The film thickness (1.2–1.5 nm) was monitored by a quartz crystal oscillator QSG 101. For decoration, gold was evaporated at 90° incidence from a tantalum wire by resistance heating. The film thickness was controlled using the microtome knife as a shutter and monitored with QSG 101. The nominal thickness of the metal deposit was ~0.2 nm, corresponding to approximately one monolayer of gold. After carbon backing the replicas were floated onto water. No further cleaning steps were necessary.

Electron micrographs were taken with a JEOL 100CX. The magnification was calibrated using ultrathin sections of muscovite crystals. Optical diffractometry was used to determine the two-dimensional lattice constants of the different crystal planes revealed by freeze-etching. Decorated crystal planes with minimal shadowing contributions and negligible lattice distortions were selected for digital image processing by visual inspection and optical diffractometry. Areas of 1024 × 1024 pixels, from micrographs taken at a magnification of 33 000× were digitized with an EIKONIX CCD camera system at a step size of 15 μm, which corresponds to a pixel size of 0.45 nm at the specimen level. The images were subjected to standard correlation averaging (CAV) procedures (Saxton and Baumeister, 1982).

Electron microscopy

For routine examination by transmission electron microscopy, purified proteasomes were negatively stained with 2% ammonium molybdate (w/v, pH 7.5). Micrographs were taken with a Philips CM 12 operated at 100 keV and a primary magnification of 36 000×.

Image processing and image simulations

Model calculations were made, representing all subunits by spheres of constant density with smoothed surfaces. Four rings of six or seven spheres were stacked together to form a cylinder 15 nm high and 11 nm in diameter. Various models were generated by changing the orientation of the individual rings with respect to each other by rotating them around the cylinder axis. For these models projections were calculated and compared with the experimentally obtained projection data to find the best match.

Acknowledgements

The authors wish to thank W.Zillig (Martinsried) for providing *T.acidophilum* cells and B.Dahlmann (Düsseldorf) for providing the purified eukaryotic proteasomes. We thank F.Zühl for preparing *T.acidophilum* proteasomes and G.Pfeifer for his help with the electron microscopy and image analysis.

References

Arrigo,A.P., Darlix,J.L., Khandjian,E.W., Simon,M. and Spahr,P.F. (1985) *EMBO J.*, **4**, 399–406.

Arrigo,A.P., Simon,M., Darlix,J.-L. and Spahr,P.F. (1987) *J. Mol. Evol.*, **25**, 141–150.

Arrigo,A.P., Tanaka,K., Goldberg,A. and Welch,W.J. (1988) *Nature*, **331**, 192–194.

Bachmann,L., Weinkauf,S., Baumeister,W., Wildhaber,I. and Bacher,A. (1989) *J. Mol. Biol.*, **207**, 575–584.

Baumeister,W., Dahlmann,B., Hegerl,R., Kopp,F., Kuehn,L. and Pfeifer,G. (1988) *FEBS Lett.*, **241**, 239–245.

Brown,M.G., Driscoll,J. and Monaco,J.J. (1991) *Nature*, **353**, 355–357.

Dahlmann,B., Kühn,L., Rutschmann,M. and Reinauer,H. (1985) *Biochem. J.*, **228**, 161–170.

Dahlmann,B., Kopp,F., Kühn,L., Niedel,B., Pfeifer,G., Hegerl,R. and Baumeister,W. (1989) *FEBS Lett.*, **251**, 125–131.

Dineva,B., Tomek,W., Köhler,K. and Schmid,H.P. (1989) *Mol. Biol. Rep.*, **13**, 207–211.

Driscoll,J. and Goldberg,A.L. (1990) *J. Biol. Chem.*, **265**, 4789–4792.

Engel,A. (1978) *Ultramicroscopy*, **3**, 273–281.

Engel,A. and Reichelt,R. (1988) *Scann. Microsc. Suppl.*, **2**, 285–293.

England,T.E. and Uhlenbeck,O.C. (1987) *Nature*, **275**, 560–561.

Eytan,E., Ganoth,D., Armon,T. and Hershko,A. (1989) *Proc. Natl. Acad. Sci. USA*, **86**, 7751–7755.

Falkenburg,P.E., Haass,C., Kloetzel,P.M., Niedel,B., Kopp,F., Kuehn,L. and Dahlmann,B. (1988) *Nature*, **331**, 190–192.

Fuijiwara,T. *et al.* (1990) *J. Biol. Chem.*, **265**, 16604–16613.

Glynne,R., Powis,S.H., Beck,S., Kelly,A., Kerr,L.A. and Trowsdale,J. (1991) *Nature*, **353**, 357–360.

Grziwa,A., Baumeister,W., Dahlmann,B. and Kopp,F. (1991) *FEBS Lett.*, **290**, 186–190.

Haass,C., Pesold-Hurt,B., Multhaupt,G., Beyreuther,K. and Kloetzel,P.M. (1990) *Gene*, **90**, 235–241.

Harris,J.R. (1968) *Biochim. Biophys. Acta*, **1500**, 534–537.

Hegerl,R., Pfeifer,G., Pühler,G., Dahlmann,B. and Baumeister,W. (1991) *FEBS Lett.*, **283**, 117–121.
Horsch,A., Martins de Sa,C., Dineva,B., Spindler,E. and Schmid,H.P. (1989) *FEBS Lett.*, **246**, 131–136.
Hough,R., Pratt,G. and Rechsteiner,M. (1988) In Rechsteiner,M. (ed.), *Ubiquitin*. Plenum, New York, pp. 101–134.
Ishiura,S., Nomura,Y., Tsukahara,T. and Sugita,H. (1989) *FEBS Lett.*, **257**, 123–126.
Kleinschmidt,J.A., Hügle,B., Grund,Ch. and Francke,W. (1983) *Eur. J. Cell Biol.*, **32**, 143–156.
Kopp,F., Steiner,R., Dahlmann,B., Kuehn,L. and Reinauer,H. (1986) *Biochim. Biophys. Acta*, **872**, 253–260.
Maniatis,T., Fritsch,E.F. and Sambrook,J. (1982) *Molecular Cloning: A Laboratory Manual*. Cold Spring Harbor Laboratory Press, Cold Spring Harbor, NY.
Monaco,J.J. and McDevitt,H.O. (1982) *Proc. Natl. Acad. Sci. USA*, **79**, 3001–3005.
Monaco,J.J. and McDevitt,H.O. (1984) *Nature*, **309**, 797–799.
Orlowski,M. (1990) *Biochemistry*, **29**, 10289–10297.
Parham,P. (1990) *Nature*, **348**, 674–675.
Rivett,J.A (1989) *Arch. Biochem. Biophys.*, **268**, 1–8.
Schägger,H. and von Jagow,G. (1987) *Anal. Biochem.*, **166**, 368–379.
Saxton,W.O. and Baumeister,W. (1982) *J. Microsc.*, **127**, 127–138.
Scherrer,K. (1990) *Mol. Biol. Rep.*, **14**, 1–9.
Schliephacke,M., Kremp,A., Schmid,H.P., Köhler,K. and Kull,U. (1991) *Eur. J. Cell Biol.*, **55**, 114–121.
Schmid,H.P., Akhayat,O., Martins de Sa,C., Puvion,F., Köhler,K. and Scherrer,K. (1984) *EMBO J.*, **3**, 29–34.
Skilton,H.E., Eperon,I.C. and Rivett,J. (1991) *FEBS Lett.*, **279**, 351–355.
Smith,P.K. *et al.* (1985) *Anal. Biochem.*, **150**, 76–85.
Tanaka,K. *et al.* (1988) *J. Mol. Biol.*, **203**, 985–996.
Wall,J.S. and Hainfield,J.F. (1986) *Annu. Rev. Biophys. Biophys. Chem.*, **15**, 355–376.
Weinkauf,S., Bacher,A., Baumeister,W., Ladenstein,R., Huber,R. and Bachmann,L. (1991) *J. Mol. Biol.*, **221**, 637–645.
Zwickl,P., Pfeifer,G., Lottspeich,F., Kopp,F., Dahlmann,B. and Baumeister,W. (1990) *J. Struct. Biol.*, **103**, 197–203.
Zwickl,P., Grziwa,A., Pühler,G., Dahlmann,B., Lottspeich,F. and Baumeister,W. (1992) *Biochemistry*, **31**, 964–972.

Received on December 20, 1991; revised on January 22, 1992